AIP Journal of Applied Physics

Effects of growth temperature on In N Ga N nanodots grown by metal organic chemical vapor deposition

Wen-Hao Chang, Wen-Cheng Ke, Shu-Hung Yu, Lin Lee, Ching-Yu Chen, Wen-Che Tsai, Hsuan Lin, Wu-Ching Chou, Ming-Chih Lee, and Wei-Kuo Chen

Citation: Journal of Applied Physics **103**, 104306 (2008); doi: 10.1063/1.2927249
View online: http://dx.doi.org/10.1063/1.2927249
View Table of Contents: http://scitation.aip.org/content/aip/journal/jap/103/10?ver=pdfcov
Published by the AIP Publishing

Articles you may be interested in

Identification of important growth parameters for the development of high quality Al x > 0.5 Ga 1 x N grown by metal organic chemical vapor deposition
J. Vac. Sci. Technol. A **25**, 441 (2007); 10.1116/1.2713409

In Ga N Ga N nanostripe grown on pattern sapphire by metal organic chemical vapor deposition
Appl. Phys. Lett. **90**, 013110 (2007); 10.1063/1.2430487

Structural and optical properties of In Ga N Ga N multiple quantum wells grown on nano-air-bridged GaN template
Appl. Phys. Lett. **89**, 171921 (2006); 10.1063/1.2372686

In -rich In 1 x Ga x N films by metalorganic vapor phase epitaxy
Appl. Phys. Lett. **85**, 6131 (2004); 10.1063/1.1842375

Ga In N Ga N growth optimization for high-power green light-emitting diodes
Appl. Phys. Lett. **85**, 866 (2004); 10.1063/1.1779960

Re-register for Table of Content Alerts

Create a profile.
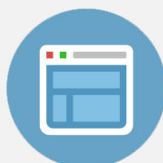
Sign up today!

[This article is copyrighted as indicated in the article. Reuse of AIP content is subject to the terms at: http://scitation.aip.org/termsconditions. Downloaded to] IP: 140.113.38.11 On: Wed, 30 Apr 2014 08:04:13

Effects of growth temperature on InN/GaN nanodots grown by metal organic chemical vapor deposition

Wen-Hao Chang,[a] Wen-Cheng Ke, Shu-Hung Yu, Lin Lee, Ching-Yu Chen, Wen-Che Tsai, Hsuan Lin, Wu-Ching Chou, Ming-Chih Lee, and Wei-Kuo Chen[b]
Department of Electrophysics, National Chiao Tung University, Hsinchu 300, Taiwan

(Received 23 November 2007; accepted 18 March 2008; published online 23 May 2008)

InN nanodots grown on GaN by metal organic chemical vapor deposition using conventional growth mode as well as flow-rate modulation epitaxy at various growth temperatures (550–730 °C) were investigated. We found that different precursor injection schemes together with the effect of growth temperatures greatly influenced the surface morphology of InN nanodots and their photoluminescence (PL) properties. The sample grown at around 650 °C showed the highest growth rate. For samples grown at higher temperatures, the residual carrier concentration was reduced and the PL efficiency was improved. Furthermore, we found that the growth of InN nanodots is still sustainable even at a temperature higher than 700 °C while retaining their optical quality. © *2008 American Institute of Physics*. [DOI: 10.1063/1.2927249]

I. INTRODUCTION

In the past few years, InN thin films with remarkably improved crystalline quality has been realized by techniques of molecular beam epitaxy[1] (MBE) as well as metal organic chemical vapor deposition (MOCVD).[2] Many experimental evidences have indicated that InN is a narrow-band-gap material with an energy gap near 0.69 eV,[3–7] rather than the previously accepted value of ~1.9 eV.[8] This finding has stimulated considerable interest, because the potential application of ternary InGaN alloys can be further extended into the near-infrared range. Besides the thin film growth, the fabrication of InN nanostructures, such as nanorods[9,10] and nanodots,[11–22] also progressed during the last few years. Such nanostructures are fascinating, since the narrow-band-gap InN combined with wide-band-gap barrier materials (such as GaN or AlN) could form a low-dimensional system with large confinement energy. During the initial stage of heteroepitaxial growth by using either MBE (Refs. 11–17) or MOCVD (Refs. 18–22), InN nanodots with controllable size and density can be formed on GaN (Refs. 11, 13–15, and 17–22) or AlN (Refs. 17 and 19) templates, or directly on Si(111) (Refs. 12 and 19) as well as nitridated sapphire[16] substrates. The nucleation process, structural properties, and even strain state of InN nanodots on various substrates have recently been investigated.[23,24] However, only a few reports addressed the optical properties.[19–21]

The growth of InN nanostructures with high crystalline quality and good optical properties for practical applications remains a great challenge. The difficulty arises not only from the large lattice mismatch between InN and the substrates, but also from the low decomposition temperature of InN.[25] It is expected to occur at 520–550 °C, resulting in a rapid escape of nitrogen atoms from the surface. If the active nitrogen is insufficient to compensate such a decomposition, surface accumulation of metallic indium will occur.[26,27] In MBE growth of InN, this problem may be partially solved by utilizing low growth temperatures, typically below 550 °C. However, the situation in MOCVD became even worse, due to the inefficient NH_3 decomposition at 600 °C and below.[25] In this regard, a higher growth temperature is preferred in the MOCVD growth of InN, in order to provide more active nitrogen. However, the growth temperature is usually limited to around 700 °C, because of the indium desorption and other high-temperature effects, such as the increase in H_2 partial pressure, which is known to significantly hinder the growth of indium-containing nitrides.[28,29]

In our previous works, we have demonstrated that InN nanodots with good optical quality can be prepared by the flow-rate modulation epitaxy (FME).[30] It is a modified growth technique of MOCVD, in which the indium and nitrogen source precursors were alternately supplied.[20,21] In this work, we further study the effects of growth temperature on the surface morphology and photoluminescence (PL) properties of InN/GaN nanodots grown by FME. In additions, InN dots grown by the conventional MOCVD method (i.e., a continuous growth mode) have also been investigated. The different morphologies of surface dots and their dependences on the growth temperature and the precursor injection scheme are discussed. PL characterization was used to evaluate the optical properties of InN nanodots. Intrinsic properties of InN nanodots, such as band gap energy, background electron concentration, and the formation of deep acceptor states, were obtained by PL line shape analysis. Our results provide valuable information for engineering the self-assembled growth of high optical quality InN nanostructures.

II. EXPERIMENTS

Samples in this study were grown on sapphire (0001) substrates in a MOCVD system using trimethylgallium (TMGa), trimethylindium (TMIn), and ammonia (NH_3) as source precursors. After nitridation of the sapphire substrate at 1120 °C, a thin GaN nucleation layer was first grown at

[a]Author to whom correspondence should be addressed. Electronic mail: whchang@mail.nctu.edu.tw.
[b]Electronic mail: wkchen@cc.nctu.edu.tw.

 © 2008 American Institute of Physics

[This article is copyrighted as indicated in the article. Reuse of AIP content is subject to the terms at: http://scitation.aip.org/termsconditions. Downloaded to] IP: 140.113.38.11 On: Wed, 30 Apr 2014 08:04:13

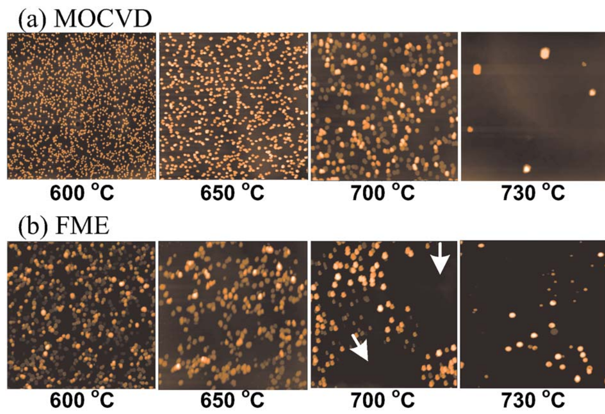

FIG. 1. (Color online) AFM images of the surface morphology of InN nanodots grown at different T_g by (a) FME and by (b) conventional MOCVD. The scanned area for each image is $10\times 10\ \mu m^2$.

520 °C, followed by the growth of an 1-μm-thick undoped GaN buffer layer at 1120 °C. The substrate temperature was then decreased to 550–730 °C to grow InN nanodots. Two sets of samples with InN dots grown by FME and conventional MOCVD growth modes have been prepared at different growth temperatures. In FME, the gas flow sequence in one growth cycle consists of four steps: a 20 s TMIn step, a 20 s NH_3 step, and two 10 s purge steps of nitrogen carrier gas intervened in between. The TMIn and NH_3 flow rates were 150 and 18 000 SCCM (SCCM denotes cubic centimeter per minute at STP), respectively. In addition, during the TMIn step, a small amount of NH_3 (with a flow rate of 1000 SCCM) was intentionally supplied in order to suppress the reevaporation of indium atoms.[21] The FME growth of InN dots were finally completed by a total of six cycles for all samples. For growing InN dots by conventional MOCVD, continuous flows of 150 SCCM TMIn and 10 000 SCCM NH_3 were supplied for 120 s. Note that the total amount of TMIn supplied in both growth methods are the same.

Surface morphologies of the InN nanodots were examined by atomic force microscopy (AFM). PL measurements were carried out at T=10 K in a cryostat using the 488 nm line of an argon-ion laser as an excitation source. The PL signals were analyzed by a 0.5 m monochomator and detected by an extended InGaAs photodiode (with a cutoff wavelength at 2.05 μm) using the standard lock-in technique.

III. RESULTS AND DISCUSSIONS

A. Growth and structural properties

Surface morphologies of the InN nanodots grown at different growth temperatures (T_g) by the conventional MOCVD and the FME methods are shown in Figs. 1(a) and 1(b), respectively. The scanned area for each AFM image is $10\times 10\ \mu m^2$. It is clear that the dot size and density are markedly influenced by the growth temperature. In general, the dot size increases whereas the dot density decreases with the increasing T_g due to the enhanced surface mobility of adatoms. As shown in Figs. 2(a) and 2(b) the shape of these InN islands is hexagonal with a truncated flat top and steep faceted sidewalls as observed typically. The average height

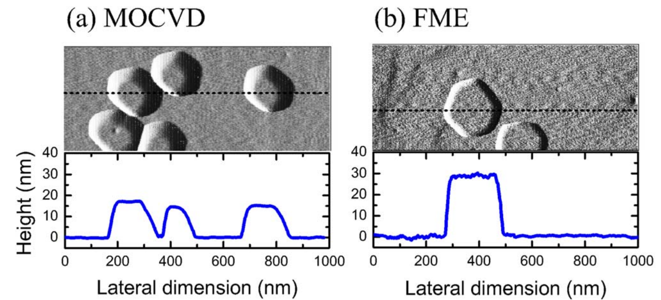

FIG. 2. (Color online) AFM images and line profiles across typical InN nanodots grown at T_g=650 °C by (a) conventional MOCVD and by (b) FME.

of FME dots increases from 11 to 30 nm as T_g was increased from 550 to 650 °C [see Fig. 3(a)]. At still higher T_g, the average height remains constant at ~30 nm. In contrast, the average height of MOCVD dots increases continuously even for $T_g>700$ °C, reaching 80 nm at 730 °C. Apart from the dot height, their base length also changes with the growth temperature, as evidenced in Fig. 3(b). It is worth to note that the aspect ratio (height-to-diameter ratio) of the InN nanodots generally increase with the increasing T_g. For MOCVD dots, the aspect ratio is typically around ~1/10 for $T_g<700$ °C and increases to ~1/4 at T_g=730 °C. On the other hand, the FME dots are flatter than MOCVD dots, with an aspect ratio of ~1/16 at T_g=550 °C and increases to ~1/8 for $T_g\geqslant 650$ °C.

The variation of dot density as a function of T_g is depicted in Fig. 4(a). For the conventional MOCVD growth, different behaviors can be clearly distinguished at about 700 °C. At lower growth temperatures ($T_g\leqslant 700$ °C), the dot density decreases gradually from 7.5×10^9 to $5.0\times 10^8\ cm^{-2}$. However, at higher growth temperatures ($T_g>700$ °C), the dot density decreases rapidly, and eventually no InN can be grown for $T_g>730$ °C. For the case of FME, the dot density also decreases with the increasing T_g, but

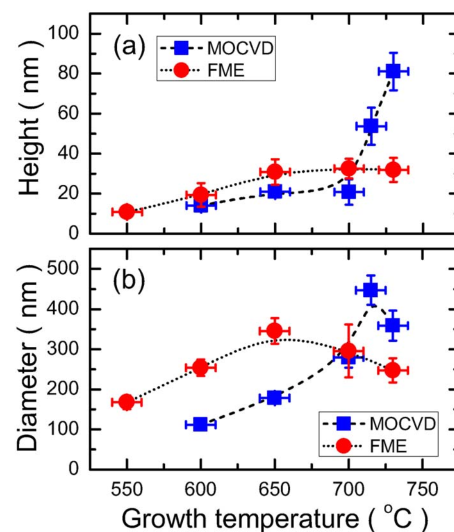

FIG. 3. (Color online) (a) The average dot height and (b) diameter of the InN nanodots grown by the FME and the conventional MOCVD methods as functions of T_g.

[This article is copyrighted as indicated in the article. Reuse of AIP content is subject to the terms at: http://scitation.aip.org/termsconditions. Downloaded to] IP: 140.113.38.11 On: Wed, 30 Apr 2014 08:04:13

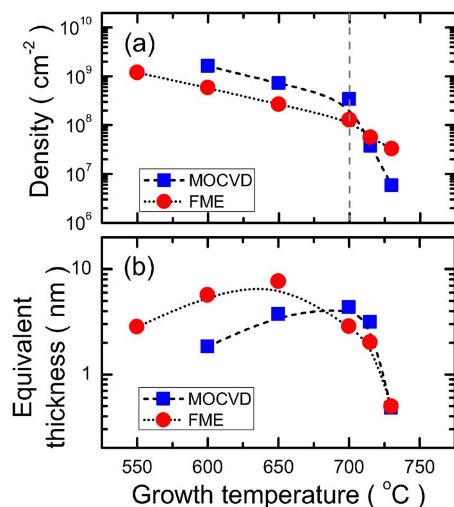

FIG. 4. (Color online) (a) The density of InN dots grown by the FME and the conventional MOCVD methods as a function of T_g. (b) The equivalent thickness of the deposited InN deduced from the dot density, the average height, and the shape of the InN dots acquired from AFM measurements.

shows a less rapid decreasing trend at growth temperatures higher than 700 °C, as compared with that of MOCVD samples.

Based on the surface morphology, the effective growth rate and its dependence on T_g can be estimated. This was done by deducing the equivalent thickness of the deposited InN from the measured average height, shape, and the density of these InN dots. Such results are plotted as function of T_g in Fig. 4(b). One can see that the highest growth rate was achieved by the FME method at T_g=650 °C, corresponding to a growth rate of ~300 nm/h. The conventional MOCVD growth shows lower growth rates in the lower temperature range and exhibits a maximum at T_g=700 °C. However, the growth rate for both methods decreases rapidly when T_g >700 °C.

The InN growth is controlled by a number of factors, such as the cracking efficiency of NH_3, the InN decomposition, as well as the indium desorption. Because these factors are temperature dependent, the different surface dot morphologies and their dependence on T_g, can be understood from the interplay among these factors together with the different precursor injection schemes used in the FME and the conventional MOCVD methods. In general, the growth process can be divided into three regimes, distinguished by differences in the surface kinetics of indium adatoms and effective In/N atomic ratio on the surface in different growth temperature ranges.

In the lower growth temperature regime (T_g<600 °C), the growth process is mainly limited by the low cracking efficiency of NH_3. The InN growth in this regime is very inefficient so that a high NH_3 flow rate (or a high V/III ratio) is usually necessary in order to prevent the formation of indium droplet. Surface morphology in this regime is characterized by very dense islands' nucleation, due to the low surface mobility of indium and nitrogen adatoms.

In the intermediate temperature regime (T_g =600–700 °C), the InN growth proceeds from dense to sparse islands' nucleation as T_g was increased, indicative of an enhanced surface kinetics of adatoms. In addition, both growth methods in this regime show an increasing growth rate with the increasing T_g. This can be attributed to a higher efficiency of NH_3 thermal cracking that provides more active nitrogen for the InN growth. However, the thermal decomposition of InN also becomes significant in this temperature range. Therefore, the InN growth in this regime becomes complicated by the competition between the forward and reverse reactions, depending on the effective In/N atomic ratio on the surface. In Fig. 4(b), we can see that the growth rate of FME method starts to decrease when T_g>650 °C, which is lower than the conventional MOCVD method occurring at 700 °C. In FME, the InN growth proceeds only in the TMIn step, during which the background NH_3 flow was kept at only 1/10 of that used in continuous growth mode. With the increasing T_g, the small amount of background NH_3 becomes unable to compensate the thermal decomposition of InN during the TMIn step, leading to a decrease in growth rate. In addition, as can be seen from the surface morphology shown in Fig. 1(a), the FME samples grown at T_g>650 °C show some void area (as indicated by arrow) that is likely to arise from the thermal decomposition of InN and subsequent reevaporation of indium during the TMIn step. On the contrary, thermal decomposition of InN is expected to be less significant in the conventional MOCVD growth for T_g ≤700 °C due to the continuous supply of a high NH_3 flow rate. However, it is worth to note that the growth rate of the conventional growth mode is slower than the FME method for T_g<700 °C. This may be a consequence of the high NH_3 flow rate, leading to parasitic gas phase reactions between hydrides and indium based metal organic compounds, especially when group III and group V precursors were simultaneously injected into the reactor.

In the high-temperature regime (T_g>700 °C), the InN growth rate decreases rapidly, regardless of how the precursors were injected. Two possible effects can explain the rapid decrease in the InN growth rate. The first one is the indium desorption, which limits the sticking of indium adatoms on the growing surface and hence prevents the InN growth. Recently, indium desorption and InN decomposition during the MBE growth of InN have been studied in detail.[26,27] However, the role of indium desorption in a MOCVD reactor is still not clear, because the growth environment is much more complex than that in a MBE system. Another one is the increase of H_2 partial pressure produced by a more efficient NH_3 thermal cracking at higher growth temperatures. It is well known that a high V/III ratio at high growth temperature will impede the growth of indium-containing nitrides, which may even lead to etching effect when a large amount of hydrogen is present.[28,29] Indeed, this is also the reason why it is not possible to grow InN using H_2 as a carrier gas.

We also found that the use of different precursor injection schemes greatly influenced the evolution of dot size with growth temperature. As shown in Fig. 3(a), the average height of FME dots tends to be saturated at T_g≥650 °C, whereas the height of MOCVD dots increases with T_g even up to 730 °C. This finding can be explained by the impact of the amount of active nitrogen on surface kinetics of indium adatoms during the nucleation of InN nanodots. In FME

[This article is copyrighted as indicated in the article. Reuse of AIP content is subject to the terms at: http://scitation.aip.org/termsconditions. Downloaded to] IP: 140.113.38.11 On: Wed, 30 Apr 2014 08:04:13

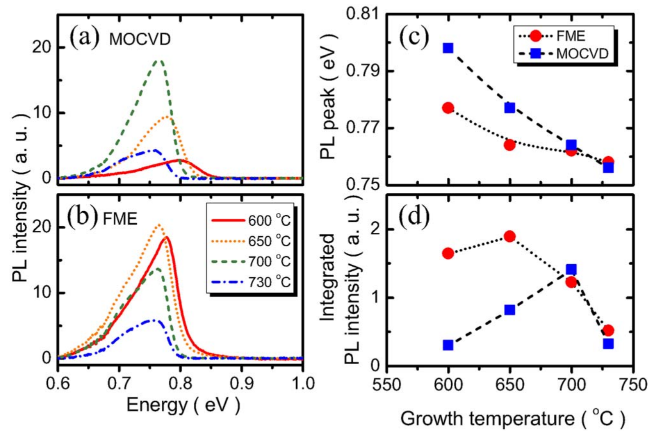

FIG. 5. (Color online) The PL spectra of InN dots grown by (a) MOCVD and (b) FME at various T_g from 600 to 730 °C. (c) and (d) are the PL peak energy and the integrated PL intensity as functions of T_g, respectively.

growth, InN decomposition is expected to be significant at high growth temperatures ($T_g \geqslant 650$ °C) due to the low NH_3 flow rate during the TMIn step. The lack of active nitrogen might hinder excess indium adatoms from moving uphill to island tops, due to the preferential formation of In-terminated surface on the InN island tops under such In-rich conditions. As a consequence, indium adatoms tend to nucleate at the edge of InN dots, yielding islands of flat shape with a limited dot height as T_g was further increased. On the contrary, because of the high NH_3 flow rate during the conventional MOCVD growth, the exposure to a large amount of active nitrogen tends to form N-stabilized surfaces on islands tops. This facilitates uphill transfer of indium adatoms to islands tops, forming dots of significantly higher aspect ratio and hence an increasing trend in dot height even for $T_g \geqslant 730$ °C.

B. Optical properties

The influence of growth temperature on PL properties of InN nanodots has also been investigated. Figures 5(a) and 5(b) displayed the PL spectra measured at 10 K for samples grown by FME and conventional MOCVD, respectively. No PL signal was observed for samples grown at 550 °C. In fact, we found that InN grown at such low temperatures usually shows some indium droplets on the surface due to the insufficient amount of active nitrogen. For samples grown at $T_g \geqslant 600$ °C, a near-infrared PL emission band becomes observable in the range of 0.76–0.80 eV. The corresponding peak energy (E_{PL}) and integrated PL intensity (I_{PL}) as a function of T_g are plotted in Figs. 5(c) and 5(d), respectively. A redshift in the PL peak with the increasing T_g can be seen for both sets of samples. The MOCVD samples show a linear decrease in peak energy from 0.80 to 0.75 eV as T_g was increased from 600 to 730 °C. For the FME samples, it generally exhibits a lower PL peak energy than that of MOCVD samples at growth temperatures in the range of $T_g = 600–700$ °C. As $T_g > 700$ °C, similar peak energies were observed for both sets of samples.

Due to the band filling effect of the degenerated electrons in the conduction band (CB), the PL peak energy E_{PL} is associated with both the band gap energy E_G of InN and the CB Fermi energy E_F with respect to the bottom of CB. At cryogenic temperatures and under low-level injections, the PL peak energy can be roughly approximated by $E_{PL} \approx E_G + E_F$, as long as the Fermi level of photogenerated holes is close to the valence band (VB) edge. The electron Fermi energy E_F is determined by the residual electron concentration (n_e) in the InN dots. On the other hand, E_G may be a function of dot height due to the size quantization effect, especially for those dots with height <20 nm. Therefore, E_G should be considered as an effective energy gap, determined by both the bulk energy gap and the confinement energy of the dots. This means that both the variation in n_e and size quantization of the InN dots have to be taken into account for the observed PL peak energy shift.

To distinguish the effects of size quantization and the variation in n_e on the PL spectra, E_G and E_F must be determined separately. We have employed a line shape model to analyze our PL spectra. The line shape model considers the recombination of degenerated electrons in the CB with photogenerated holes bound to VB tail states and/or acceptor states.[31,32] The CB nonparabolicity, the energy-dependent CB density of states, as well as the corresponding electron effective mass are calculated in the framework of Kane's two-band $\mathbf{k}\cdot\mathbf{p}$ model.[33] The energy parameter E_P of the $\mathbf{k}\cdot\mathbf{p}$ model was chosen to be $E_P = 10$ eV, corresponding to an electron effective mass of $m_e^* \approx 0.065 m_0$ at the bottom of the CB.[33] The electron concentration n_e is considered as a fitting parameter, so that E_F can be calculated from the CB dispersion at the Fermi wave vector $k_F = (3\pi^2 n_e)^{1/3}$. The band tail is also determined from n_e by calculating the root mean square of the fluctuated potential produced by ionized impurities.[31,34] In the past few years, line shape models with different levels of sophistication have been developed and utilized to analyze the PL spectra of InN.[5,10,31,32,35] However, because our main interest is to find E_G and E_F of different samples, the lineshape analysis was further simplified by assuming a deltalike function for the energy distribution of photogenerated holes near the VB edge. In this way, the line shape of the PL emission band is approximated by the electron energy distribution in the CB. The simulated line shapes together with the measured spectra are shown in Fig. 6(a) and 6(b). The simplified model is able to give a reasonable approximation to the shape of PL spectra, especially for those MOCVD samples grown at $T_g < 700$ °C. However, for the MOCVD samples grown at $T_g > 700$ °C and those FME sample grown at $T_g > 650$ °C, we found that their PL spectra exhibit a low-energy shoulder (A2) at about 50–60 meV below the main PL peak (A1), which cannot be described by the model considering only one recombination path. According to Arnaudov *et al.*,[31] and Klochikhin *et al.*,[32] the low-energy shoulder might be attributed to the recombination of degenerated electrons with a deeper acceptor state, as shown schematically in Fig. 6(c). When we included a deep acceptor state with a binding energy of $E_{A2} = 55 \pm 5$ meV, good line shape fittings can be obtained.

The fitting parameters E_G and n_e and the corresponding E_F are listed in Table I, where the corresponding average dot heights are also included for comparison. The fitted value of

[This article is copyrighted as indicated in the article. Reuse of AIP content is subject to the terms at: http://scitation.aip.org/termsconditions. Downloaded to] IP: 140.113.38.11 On: Wed, 30 Apr 2014 08:04:13

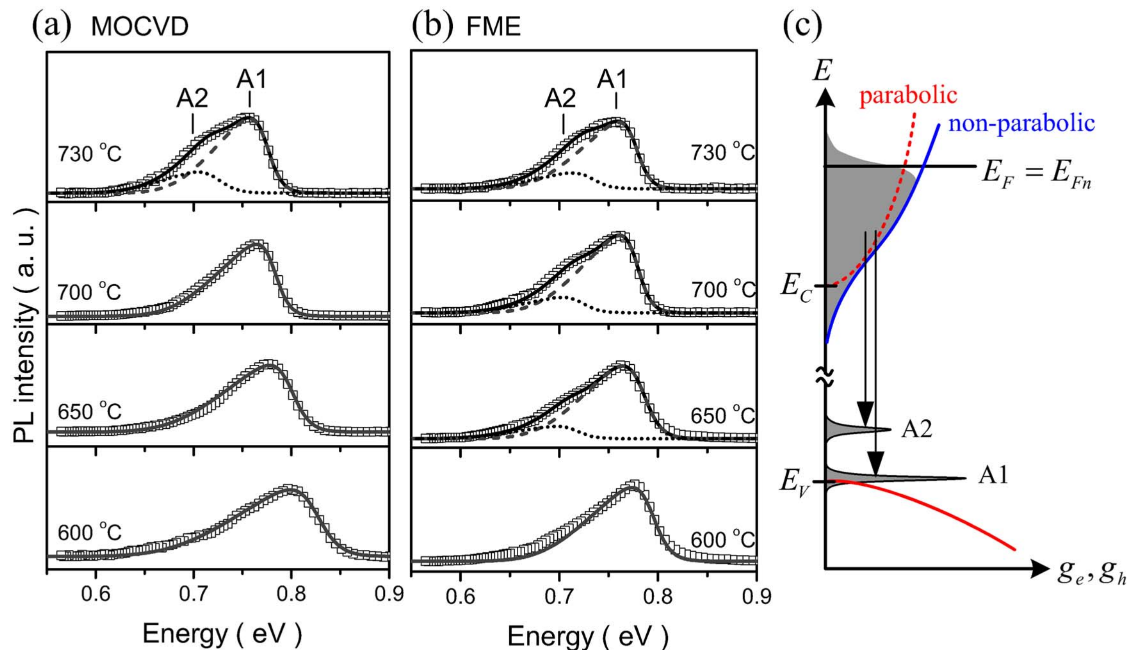

FIG. 6. (Color online) Line shape fitting for the PL spectra of the (a) MOCVD and (b) FME samples. Symbols are experimental data, while the contributions from the recombination to the VB edge state (A1 peak) and the deeper acceptor state (A2 peak) are shown by dashed and dotted lines, respectively. The sums of the two recombination paths are indicated by the black solid curves. Gray solid curves means that only one recombination path was considered. (c) A schematic diagram for illustrating the recombination paths of different acceptor levels.

E_G, which lies in the range of 0.688–0.699 eV, agrees very well with the reported values.[5,10,31,32,35] It is worth to note that E_F is very sensitive to the variation in n_e. For the MOCVD samples, the shift in E_F is nearly ~50 meV, even though the variation in n_e is still in the same order of magnitude (from 4.3×10^{18} to 2.0×10^{18} cm^{-3}). In contrast to the large shift in E_F, the variation in E_G is only about ~10 meV. This implies that the PL peak energy shift is mainly contributed from the variation in electron concentration, whereas the size quantization effect is not significant for the investigated dot heights. Indeed, the fitted values of E_G show a slightly increasing trend with the decreasing height. However, the variation in the effective gap cannot be attributed solely to the size quantization effect, because some other effects on bulk energy gap, such as the band-gap renormalization[33] (caused by the electron-electron and electron-impurity interactions) and the energy position of photogenerated holes localizing in the VB tail states,[31,36] are also incorporated into the value of E_G in the simplified model. These effects are expected to reduce the bulk energy gap somewhat and hence counteract the size quantization effect on the fitted value of E_G.

The electron concentration n_e obtained from line shape fittings for both sample sets are plotted as function of T_g in Fig. 7(a). In both cases, the background electron concentration in InN can be reduced by using a higher growth temperature, most likely related to a more efficient cracking of NH_3. The FME samples generally show a lower n_e than those grown by MOCVD for $T_g < 700$ °C, but approach nearly the same n_e for $T_g > 700$ °C. Since the NH_3 flow rate used in the conventional MOCVD method is considerably higher than that used during the TMIn step of FME, it can be inferred that the relatively higher n_e in MOCVD samples is likely to arise from the use of a high NH_3 flow rate. Similar effects have been observed in our previous study of FME grown InN dots,[21] where the use of a high NH_3 background flow always accompanied a high n_e in InN dots. Apart from the background carrier concentration, the contribution of the deep acceptor state to the PL spectrum also depends on T_g. As shown in Fig. 6, the low-energy shoulder appears in MOCVD samples for $T_g > 700$ °C and in FME samples for $T_g > 650$ °C, and becomes intense with the increasing T_g. Interestingly, by comparing the PL spectra with the deposited

TABLE I. The fitting parameters (E_G, n_e, and E_F) used in PL line shape fitting. The average dot heights for different samples are also shown for comparison.

	FME				MOCVD			
T_g (°C)	Dot height (nm)	E_g (eV)	E_F (meV)	n_e ($\times10^{18}$ cm^{-3})	Dot height (nm)	E_g (eV)	E_F (meV)	n_e ($\times10^{18}$ cm^{-3})
600	19.3	0.699	94	2.6	14.5	0.697	128	4.3
650	30.8	0.695	88	2.3	20.9	0.694	105	3.1
700	32.5	0.694	83	2.1	20.8	0.694	88	2.3
730	31.8	0.693	83	2.1	81.1	0.688	81	2.0

[This article is copyrighted as indicated in the article. Reuse of AIP content is subject to the terms at: http://scitation.aip.org/termsconditions. Downloaded to] IP: 140.113.38.11 On: Wed, 30 Apr 2014 08:04:13

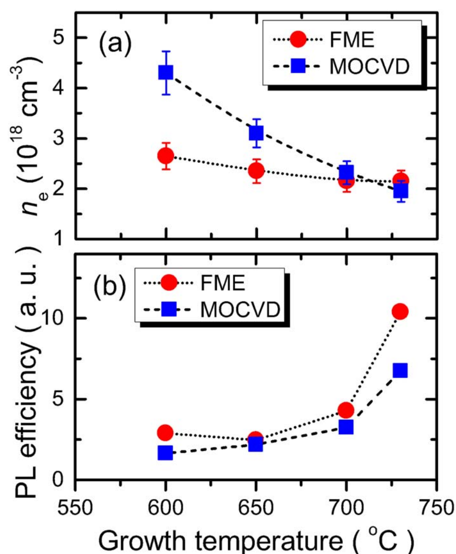

FIG. 7. (Color online) (a) The deduced electron concentrations n_e from line shape model for both set of samples. (b) The PL efficiency as function of T_g. The PL efficiency is obtained by normalizing the measured PL intensity to the amount of deposited InN.

InN amount shown in Fig. 4(b), one can see that the low-energy shoulder appears when the InN growth rate starts to decrease. Although we are not able to identify the species of the deep acceptor state at current stage, it is clear that the deep acceptor state originated from the high-temperature growth, most likely related to indium desorption and other high-temperature effects that hinder the incorporation of indium into the growing surface. Indium vacancies (V_{In}) or their related defects arising from the lack of indium species are possible candidates for the deep acceptor state. Recently, the V_{In} concentration in MOCVD-grown InN film determined by positron annihilation measurements was also found to increase with the increasing growth temperature.[37] This experimental finding seems to support our assignment of the low-energy shoulder in PL spectra to the formation of V_{In} related defects.

Regarding the PL efficiency of the InN nanodots, a high PL efficiency usually indicates a good material quality with reduced nonradiative recombination centers. In Fig. 5(d), one can see that the integrated PL intensity as a function of T_g shows a general correlation with the amount of deposited InN plotted in Fig. 4(b). In order to evaluate the PL efficiency of different samples, the integrated PL intensity was normalized to the amount of deposited InN, which is shown as a function of T_g in Fig. 7(b). One can see that a higher PL efficiency can be achieved by using a higher T_g for both growth methods. Furthermore, with the increasing T_g, the increase in PL efficiency is found to be larger than the decrease in n_e as evidenced in Figs. 7(a) and 7(b). For a dominant Auger recombination process, the PL efficiency is expected to have a $1/n_e$ dependence. Therefore, the large increase in PL efficiency reflects that such an improvement in PL efficiency arises not only from the reduced n_e, but also from the reduced nonradiative recombination centers.

Before concluding, we would like to remark on some relevant features with regard to the growth optimization of InN dots. In our previous work,[21] we have demonstrated that the size, shape, and density of the InN dots can be controlled by using different NH_3 background flows in the FME growth. In this study, as has been discussed in the Sec. III A, it is clear that the growth temperature is also an important parameter for engineering the self-assembled growth of InN nanostructures. Therefore, by optimizing both parameters, i.e., the growth temperature and the NH_3 flow rate, it is possible to control the size and density of the InN dots independently, in the range with surface density ranging from 6×10^6 to 1×10^{10} cm^{-2}. In the context of realizing high intensity light emitters using InN dots as an active material, the growth of small and high density InN dots is very important. In general, a higher dot density can be achieved by a lower growth temperature and a higher NH_3 flow rate. However, InN dots grown under such conditions usually show inferior optical properties. For practical applications, a compromise between the optical quality and the structural properties seems to be inevitable. Recently, Ruffenach *et al.*[22] demonstrated that the surface density of InN dots can be further controlled by using different rare gases as a carrier gas. A very high dot density (5×10^{10} cm^{-2}) was achieved by replacing the nitrogen carrier gas by argon. Although the influence of rare gases on the optical property of InN dots is still unclear, this method may provide a different approach to achieve both high density and high optical quality InN dots.

IV. CONCLUSIONS

InN/GaN nanodots grown by the FME and conventional MOCVD methods have been investigated. The characteristic size, density, and shape of InN dots were greatly influenced by the growth temperature together with the precursor injection schemes. In terms of their optical quality, the growth temperature range for InN nanodots was found to be T_g =600–730 °C. For $T_g \leqslant 700$ °C, higher growth rate can be achieved at a lower growth temperature by the FME method than the conventional MOCVD growth, due possibly to the alternate injection of group III and group IV precursors, which might mitigate the parasitic gas phase reactions. The optimal growth rate was achieved by the FME method at T_g=650 °C. For $T_g > 700$ °C, the growth of InN by both methods is still sustainable while retaining its optical quality, but at the expense of a very low growth rate. The effects of growth temperature on intrinsic properties of InN nanodots were studied, in which the effective band gap energy and the residual electron concentration were obtained by PL line shape analysis. We found that the incorporation of deep acceptor states became more severe at a higher growth temperature, which might relate to the formation of In vacancies or their related defects. Our results also suggest that a higher growth temperature is beneficial for both reducing the residual carrier concentration and enhancing the PL efficiency of the InN dots.

ACKNOWLEDGMENTS

This work is supported in part by the project of MOE-ATU and the National Science Council of Taiwan under Grant Nos. NSC 96-2112-M-009-006, NSC 95-2112-M-009-

[This article is copyrighted as indicated in the article. Reuse of AIP content is subject to the terms at: http://scitation.aip.org/termsconditions. Downloaded to] IP: 140.113.38.11 On: Wed, 30 Apr 2014 08:04:13

044-MY3, NSC 96-2112-M-009-026-MY3, and NSC 96-2112-M-009-014.

[1]H. Lu, W. J. Schaff, J. Hwang, H. Wu, G. Koley, and L. F. Eastman, Appl. Phys. Lett. **79**, 1489 (2001).
[2]A. Yamamoto, T. Tanaka, K. Koide, and A. Hashimoto, Phys. Status Solidi A **194**, 510 (2002).
[3]V. Yu. Davydov, A. A. Klochikhin, R. P. Seisyan, V. V. Emtsev, S. V. Ivanov, F. Bechstedt, J. Furthmüller, H. Harima, A. V. Mudryi, J. Aderhold, O. Semchinova, and J. Graul, Phys. Status Solidi B **229**, R1 (2002).
[4]V. Yu. Davydov, A. A. Klochikhin, V. V. Emtsev, S. V. Ivanov, V. V. Vekshin, F. Bechstedt, J. Furthmüller, H. Harima, A. V. Mudryi, A. Hashimoto, A. Yamamoto, J. Aderhold, J. Graul, and E. E. Haller, Phys. Status Solidi B **230**, R4 (2002).
[5]V. Yu. Davydov, A. A. Klochikhin, V. V. Emtsev, D. A. Kudrykov, S. V. Ivanov, V. A. Vekshin, F. Bechstedt, J. Furthmüller, J. Aderhold, J. Graul, A. V. Mudryi, H. Harima, A. Hashimoto, A. Yamamoto, and E. E. Haller, Phys. Status Solidi B **234**, 787 (2002).
[6]J. Wu, W. Walukiewicz, K. M. Yu, J. W. Ager III, E. E. Haller, H. Lu, W. J. Schaff, Y. Saito, and Y. Nanishi, Appl. Phys. Lett. **80**, 3967 (2002).
[7]T. Matsuoka, H. Okamoto, M. Nakao, H. Harima, and E. Kurimoto, Appl. Phys. Lett. **81**, 1246 (2002).
[8]T. L. Tansley and C. P. Foley, J. Appl. Phys. **59**, 3941 (1986).
[9]C.-H. Shen, H.-Y. Chen, H.-W. Lin, S. Gwo, A. A. Klochikhin, and V. Yu. Davydov, Appl. Phys. Lett. **88**, 253104 (2006).
[10]T. Stoica, R. J. Meijers, R. Calarco, T. Richter, E. Sutter, and H. Luth, Nano Lett. **6**, 1541 (2006); T. Stoica, R. Meijers, R. Calarco, T. Richter, and H. Luth, J. Cryst. Growth **290**, 241 (2006).
[11]C. Nörenberg, R. A. Oliver, M. G. Martin, L. Allers, M. R. Castell, and G. A. D. Briggs, Phys. Status Solidi A **194**, 536 (2002).
[12]C. Nörenberg, M. G. Martin, R. A. Oliver, M. R. Castell, and G. A. D. Briggs, J. Phys. D **35**, 615 (2002).
[13]Y. F. Ng, Y. G. Cao, M. H. Xie, X. L. Wang, and S. Y. Tong, Appl. Phys. Lett. **81**, 3960 (2002).
[14]Y. G. Cao, M. H. Xie, Y. Liu, Y. F. Ng, H. S. Wu, and S. Y. Tong, Appl. Phys. Lett. **83**, 5157 (2003).
[15]A. Yoshikawa, N. Hashimoto, N. Kikukawa, S. B. Che, and Y. Ishitani, Appl. Phys. Lett. **86**, 153115 (2005).
[16]Y. E. Romanyuk, R.-G. Dengel1, L. V. Stebounova, and S. R. Leone, J. Cryst. Growth **304**, 346 (2007).
[17]C.-H. Shen, H.-W. Lin, H.-M. Lee, C.-L. Wu, J.-T. Hsu, and S. Gwo, Thin Solid Films **494**, 79 (2006).
[18]O. Briot, B. Maleyre, and S. Ruffenach, Appl. Phys. Lett. **83**, 2919 (2003).
[19]S. Ruffenach, B. Maleyre, O. Briot, and B. Gil, Phys. Status Solidi C **2**, 826 (2005).
[20]W. C. Ke, C. P. Fu, C. Y. Chen, L. Lee, C. S. Ku, W. C. Chou, W.-H. Chang, M. C. Lee, W. K. Chen, W. J. Lin, and Y. C. Cheng, Appl. Phys. Lett. **88**, 191913 (2006).
[21]W. C. Ke, L. Lee, C. Y. Chen, W. C. Tsai, W.-H. Chang, W. C. Chou, M. C. Lee, W. K. Chen, W. J. Lin, and Y. C. Cheng, Appl. Phys. Lett. **89**, 263117 (2006).
[22]S. Ruffenach, O. Briot, M. Moret, and B. Gil, Appl. Phys. Lett. **90**, 153102 (2007).
[23]L. Zhou, T. Xu, D. J. Smith, and T. D. Moustakas, Appl. Phys. Lett. **88**, 231906 (2006).
[24]J. G. Lozano, A. M. Sánchez, R. García, D. González, D. Araújo, S. Ruffenach, and O. Briot, Appl. Phys. Lett. **87**, 263104 (2005).
[25]For a review, see, for example, A. G. Bhuiyan, A. Hashimoto, and A. Yamamoto, J. Appl. Phys. **94**, 2779 (2003).
[26]E. Dimakis, E. Iliopoulos, K. Tsagaraki, Th. Kehagias, Ph. Komninou, and A. Georgakilas, J. Appl. Phys. **97**, 113520 (2005).
[27]C. S. Gallinat, G. Koblmüller, J. S. Brown, and J. S. Speck, J. Appl. Phys. **102**, 064907 (2007).
[28]E. L. Piner, M. K. Behbehani, N. A. El-Masry, F. G. McIntosh, J. C. Roberts, K. S. Boutros, and S. M. Bedair, Appl. Phys. Lett. **70**, 461 (1997).
[29]A. Koukitu, T. Taki, N. Takahashi, and H. Seki, J. Cryst. Growth **197**, 99 (1999).
[30]N. Kobayashi, T. Makimoto, and Y. Horikoshi, Jpn. J. Appl. Phys., Part 2 **24**, L962 (1985); Y. Horikoshi, J. Cryst. Growth **201/202**, 150 (1999).
[31]B. Arnaudov, T. Paskova, P. P. Paskov, B. Magnusson, E. Valcheva, B. Monemar, H. Lu, W. J. Schaff, H. Amano, and I. Akasaki, Phys. Rev. B **69**, 115216 (2004).
[32]A. A. Klochikhin, V. Yu. Davydov, V. V. Emtsev, A. V. Sakharov, V. A. Kapitonov, B. A. Andreev, H. Lu, and W. J. Schaff, Phys. Rev. B **71**, 195207 (2005).
[33]J. Wu, W. Walukiewicz, W. Shan, K. M. Yu, J. W. Ager III, E. E. Haller, H. Lu, and W. J. Schaff, Phys. Rev. B **66**, 201403 (2002).
[34]B. I. Shklovskii and A. L. Efros, *Electronic Properties of Doped Semiconductors* (Springer-Verlag, Berlin, 1984), Chap. 11.
[35]E. Valcheva, S. Alexandrova, S. Dimitrov, H. Lu, and W. J. Schaff, Phys. Status Solidi A **203**, 75 (2006).
[36]B. G. Arnaudov, V. A. Vilkotskii, D. S. Domanevskii, S. K. Evtimova, and V. D. Tkachev, Sov. Phys. Semicond. **11**, 1054 (1977).
[37]A. Pelli, K. Saarinen, F. Tuomisto, S. Ruffenach, and O. Briot, Appl. Phys. Lett. **89**, 011911 (2006).

[This article is copyrighted as indicated in the article. Reuse of AIP content is subject to the terms at: http://scitation.aip.org/termsconditions. Downloaded to] IP: 140.113.38.11 On: Wed, 30 Apr 2014 08:04:13